



**HAL**  
open science

# Absorbing boundary conditions for water wave simulation in the vicinity of a solid body

Jose M. Orellana

► **To cite this version:**

Jose M. Orellana. Absorbing boundary conditions for water wave simulation in the vicinity of a solid body. 2021. hal-02962100v5

**HAL Id: hal-02962100**

**<https://hal.science/hal-02962100v5>**

Preprint submitted on 29 May 2021

**HAL** is a multi-disciplinary open access archive for the deposit and dissemination of scientific research documents, whether they are published or not. The documents may come from teaching and research institutions in France or abroad, or from public or private research centers.

L'archive ouverte pluridisciplinaire **HAL**, est destinée au dépôt et à la diffusion de documents scientifiques de niveau recherche, publiés ou non, émanant des établissements d'enseignement et de recherche français ou étrangers, des laboratoires publics ou privés.



---

# Absorbing boundary conditions for water wave simulation in the vicinity of a solid body

José Marie Orellana<sup>a</sup>

<sup>a</sup> Laboratoire de modélisation mathématique et numérique (M2N), Conservatoire national des Arts et Métiers, 292, rue Saint Martin 75141 PARIS Cedex 03 France

E-mail: jose.orellana@lecnam.net (J.M. Orellana)

**Abstract.** In this paper, we focus on the modelling of the wake of a solid body moving through a body of water. To this end, the flow of an inviscid, barotropic and compressible fluid around the solid body regarded as motionless is examined. The dynamic behavior of the fluid is analyzed by means of a two-dimensional Neumann-Kelvin's coupled model enhanced with capillarity and inertia terms. For computational purposes, the unbounded spatial domain has to be truncated by artificial boundaries and appropriate absorbing boundary conditions have to be introduced. Numerous difficulties arise in dealing with short wavelength wave propagation in a stratified convective fluid media with significant differences between layer properties. Numerical illustrations of the results are given and commented.

**Keywords.** Absorbing boundary condition, fluid-structure interaction, water waves propagation, numerical simulations.

**2020 Mathematics Subject Classification.** 76N99.

This article is a draft (not yet accepted!)

## Version française abrégée

Afin de déterminer le sillage d'un corps en mouvement dans une étendue d'eau, on considère l'écoulement d'un fluide non visqueux, barotrope et compressible autour de celui-ci. On étudie la propagation d'une petite perturbation dans ce milieu considéré comme un fluide stratifié en mouvement quasi uniforme à l'aide d'un modèle couplé de type Neumann-Kelvin tenant compte de la capillarité et de l'inertie de la surface du fluide. Pour réaliser la simulation numérique, il est nécessaire de délimiter artificiellement le domaine et d'introduire des conditions aux limites absorbantes adaptées. De nombreuses difficultés apparaissent car il s'agit de traiter un problème de propagation d'ondes courtes dans un milieu fluide convectif stratifié présentant de grandes différences de propriétés entre couches. Les résultats obtenus sont analysés et commentés.

## 1. Introduction

Understanding wave propagation mechanisms on a body of water has long been an interesting topic for many researchers [1–7]. Surface water wave phenomenon is due to the balance between the gravity forces that keep horizontal free surface of the water, the surface tension that keeps

the consistency of the air-water interface, the water inertia and the difference between air and water pressures. According to the relevant effect that forces the motion, the waves are usually divided in gravity waves, capillary waves or pressure waves. In this work, the waves of interest are the surface waves generated by the movement of a solid body, that propagate all around it and interact with its rigid surface leading to a wake in its vicinity [8–10]. Unlike common approaches where the water body is viewed as a homogeneous propagating medium [3–7], here it is considered as a stratified structure [11–13]. In addition to better encompass the properties of the propagating waves, a two dimensional Neumann-Kelvin's coupled model enhanced with capillarity and inertia terms is proposed [14–16]. A straightforward method of dealing with such a scattering problem is to consider the whole unbounded structure, introduce an assumed known form of the solution, as time harmonic or even a plane wave, and apply analytically radiation boundary conditions to the solution at infinity. [3–6, 8]. In addition to these analytical methods, numerically techniques such as boundary element method [17] or finite element method with infinite elements have been developed to deal with the same formulated problem [18, 19]. Otherwise, the given domain is truncated by artificial boundaries in order to use a more classical finite element based approach along with High Order Absorbing Boundary Conditions [20–23] or Perfectly Matched Layer method [24–26]. The main concerns are then to avoid the occurrence of spurious reflection waves at boundaries and to ensure that an accurate approximation of solution on the infinite domain is obtained in the bounded one. These methods generally turn out to be quite efficient but at the cost of a more complex formulation of the problem and of a large number of variables together with calculations involved [27, 28]. Moreover, when dealing with short wavelength waves as in our case ( $\lambda \approx 10^{-2}$  m), a fine mesh is required to reduce the dispersion error and obtain numerical solutions with a acceptable accuracy, which makes the numerical resolution effort quickly prohibitive [29, 30]. Hence in the following, an approximate low order absorbing boundary condition is ideally sought not to increase these already existing costs. After stating the problem and specifying underlying assumptions, a linearization around a steady state is performed and different accurate boundary conditions are introduced to carry out the study. The variational formulation of the problem is deduced and a finite element approximation in space with a centered finite difference scheme in time are used to approach the solution. Results obtained are illustrated and discussed.

## 2. Problem statement

Our purpose is to determine the dynamical behavior of the water surface in the vicinity of a solid body that moves with an horizontal velocity  $U$  and with a possible oscillatory displacement. To this end, we examine the irrotational and inviscid flow of a compressible and barotropic fluid around the structure seen as fixed. Due to the existence of singularities at contact points between solid body surface and the surface of water, and also at underwater angular points [31], the structure is immersed and its shape is simplified to a cylinder. We consider as computational domain a rectangular open domain  $\Omega$  with a hole of radius  $R$  in its center. Its boundary  $\partial\Omega = \Gamma_0 \cup \Gamma_1 \cup \Gamma_s \cup \Gamma_2 \cup \Gamma_b$  has unit outward normal vector  $\nu$ .  $\Gamma_0$  corresponds to the bottom of the system,  $\Gamma_s$ , to the free surface of the water,  $\Gamma_1$  and  $\Gamma_2$ , to the sides through which the water flow enters and leaves  $\Omega$  and  $\Gamma_b$ , to the rigid body surface (see figure 1).  $\partial\Gamma_s$  denotes the edges of  $\Gamma_s$ . A steady flow passes through  $\Omega$  with horizontal velocity  $Ue_1$  and a small disturbance is introduced in the fluid as an initial condition.

## 3. Theoretical modelling

A common theoretical formulation of this problem consists in finding for an irrotational flow of an homogeneous and incompressible fluid, the velocity potential  $\Phi$  satisfying the classic

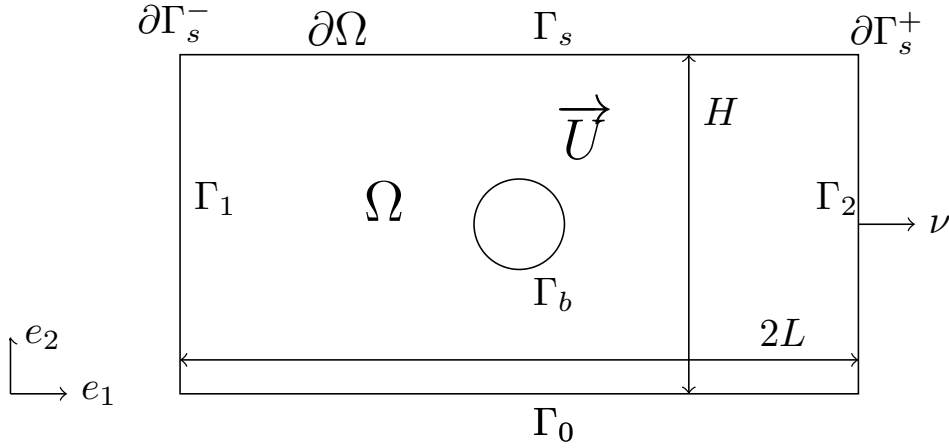


**Figure 1.** Geometry and notations of the problem.

Laplace's equation and the vertical displacement of the surface  $\eta$  verifying [11, 32–34] :

- The kinematic boundary conditions

$$\frac{\partial \Phi}{\partial \nu} = U \cdot \nu \text{ on } \Gamma_0 \cup \Gamma_b \times ]0, T[, \quad (1)$$

$$\frac{\partial \Phi}{\partial \nu} = \frac{\partial \eta}{\partial t} + \nabla_s \Phi \cdot \nabla_s \eta \text{ on } \Gamma_s \times ]0, T[. \quad (2)$$

- The dynamic boundary conditions

$$-\frac{\partial \Phi}{\partial t} - \frac{1}{2} \|\nabla_s \Phi\|^2 - g\eta + \frac{\sigma \Delta_s \eta}{\rho} = 0 \text{ on } \Gamma_s \times ]0, T[, \quad (3)$$

the subscript  $s$  indicates that the differential operator is considered locally along a surface namely here  $\Gamma_s$ .

- The radiation boundary conditions based on the behavior of the solution in the neighborhood of infinity to ensure uniqueness of the solution,

$$\nabla \Phi \rightarrow |U| \text{ as } |x_1| \rightarrow \infty, t \in ]0, T[. \quad (4)$$

Incompressibility of the flow is assumed since the water for flow speeds much smaller than the sound speeds in the water. Capillarity and gravity effects on the surface are introduced in Eq.(3) respectively by  $\sigma$  the surface tension and  $g$  the acceleration of gravity. The inertia of the surface is neglected. Under the small displacement theory assumption, a comprehensive analysis of harmonic plane wave propagation is performed dividing the wave pattern in two cases depending on steady stream velocity value [32, 33]. In the following, the propagating medium is regarded as a stratified compressible fluid waveguide with a convective uniform mean flow subject to a Gaussian pulse. Therefore the previous governing partial differential equations and resolving approach have to be revised.

### 3.1. Hypotheses and formulation of the global model

The propagating medium considered consists of two liquid layers with very different properties. The upper layer is the free surface water with an infinitesimal thickness and small characteristic

velocity of wave propagation, namely riddle or ripple velocity. The lower layer is the inner water with a finite or semi infinite thickness and with a high characteristic velocity of wave propagation, namely the speed of sound in water. Therefore two different models have to be introduced to take these features into account : an inner fluid model and a surface model.

### 3.1.1. Formulation of the inner fluid model

We assume that the flow is characterized by two variables modelling the mass density  $\rho_{tot}$  and the velocity potential  $\Phi$  that satisfy :

- The conservation of mass equation

$$\frac{\partial \rho_{tot}}{\partial t} + div(\rho_{tot} \nabla \Phi) = 0 \text{ in } \Omega \times ]0, T[. \quad (5)$$

- The Bernoulli equation for unsteady compressible potential flow (neglecting gravity effect)

$$\frac{\partial \Phi}{\partial t} + \frac{1}{2} \|\nabla \Phi\|^2 + F(\rho_{tot}) = 0 \text{ in } \Omega \times ]0, T[ \quad (6)$$

where  $F(\rho_{tot}) = \int_{\rho_0}^{\rho_{tot}} \frac{1}{\rho} \cdot \frac{\partial p}{\partial \rho} d\rho + F(\rho_0)$  is the barotropic potential,  $p$ , the fluid pressure and  $T$ , the simulation time.

### 3.1.2. Formulation of the surface model

Applying Newton's second law of motion to an infinitesimal small surface element of thickness  $2\varepsilon$  that vertically moves of a displacement  $\eta_{tot}$ , leads to the free surface equilibrium equation :

$$2\varepsilon \rho_{tot} \frac{D^2 \eta_{tot}}{Dt^2} = -\rho_{tot} \frac{\partial \Phi}{\partial t} - \frac{\rho_{tot}}{2} \|\nabla_s \Phi\|^2 + \sigma \Delta_s \eta_{tot} - \rho_{tot} g \eta_{tot} \text{ in } \Gamma_s \times ]0, T[ \quad (7)$$

where the forces involved consist in the capillary action  $\sigma \Delta_s \eta_{tot}$ , the gravity force  $-\rho_{tot} g \eta_{tot}$  and the pressure  $-\rho_{tot} \partial \Phi / \partial t - \rho_{tot} \|\nabla_s \Phi\|^2 / 2$ . From a mathematical point of view, capillary term stabilizes the partial differential equation [16].

### 3.1.3. On the interface

The kinematic boundary condition Eq.(2) becomes the continuity of normal velocity at the interface :

$$\frac{\partial \eta_{tot}}{\partial t} + \nabla_s \Phi \cdot \nabla_s \eta_{tot} = \frac{\partial \Phi}{\partial v} \text{ in } \Gamma_s \times ]0, T[ \quad (8)$$

taking account of the rotation of the normal to the surface.

## 3.2. Linearization of the governing equations

The global nonlinear dynamical model obtained is linearized around a main steady state. Therefore the global solution is split into the steady state obtained and a transient one. The lateral boundary conditions are defined separately according to the nature of the state. For the steady flow, the most realistic condition is to fix the normal velocity. For transient flow, non-reflecting boundary conditions have to be prescribed for the inlet and the outlet of  $\Omega$  in order to avoid any spurious reflections of the waves reaching the boundaries of the domain.

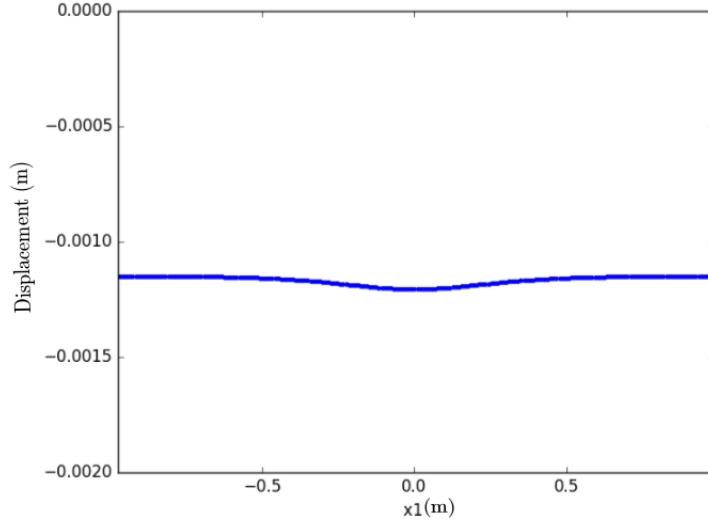


**Figure 2.** Free surface vertical displacement  $\eta_0$  (m) solution of Eq.(10) versus  $x_1$  (m) with the ‘digging’ effect.

### 3.2.1. Main background steady state flow

We introduce  $\varphi_0$ , the velocity potential corresponding to a steady quasi uniform horizontal steady flow of an incompressible fluid which enters and leaves  $\Omega$  at constant unit horizontal velocity with normal surface displacement variation along  $\Gamma_s$  regarded as negligible and non penetrability condition on  $\Gamma_0 \cup \Gamma_b$  satisfied. This background flow is stationary with respect to the boat which is chosen as frame of reference.  $\varphi_0$  is the solution to the following problem :

$$\begin{cases} -\Delta\varphi_0 = 0 \text{ in } \Omega \text{ and } \int_{\Gamma_s} \varphi_0 = 0, \\ \frac{\partial\varphi_0}{\partial\nu} = 0 \text{ on } \Gamma_0 \cup \Gamma_b \cup \Gamma_s, \\ \frac{\partial\varphi_0}{\partial\nu} = (e_1 \cdot \nu) \text{ in } \Gamma_1 \cup \Gamma_2. \end{cases} \quad (9)$$

To obtain the related displacement on the surface  $\eta_0$  of this flow for our model, stationary balance of forces on free surface Eq.(7) along with homogeneous Neumann boundary conditions are applied. According to the frame of reference, it leads in stationary case to :

$$\begin{cases} 2\varepsilon\rho_0U^2\nabla_s\varphi_0 \cdot \nabla_s(\nabla_s\varphi_0 \cdot \nabla_s\eta_0) + \sigma\Delta_s\eta_0 - \rho_0g\eta_0 = -\frac{\rho_0}{2}U^2\|\nabla_s\varphi_0\|^2 \text{ in } \Gamma_s, \\ \frac{\partial\eta_0}{\partial\nu_s} = 0 \text{ on } \partial\Gamma_s \end{cases} \quad (10)$$

with  $\rho_0$ , the fluid density and  $g$ , the gravity acceleration. The solution of Eq.(9) corresponds to a steady quasi uniform horizontal flow with a digging effect due to the term  $-\rho_0U^2\|\nabla_s\varphi_0\|^2/2$  as shown in figure 2. The order of magnitude of free surface strain is about  $10^{-3}m$  and therefore negligible in comparison with initial computational domain  $\Omega$  dimensions.

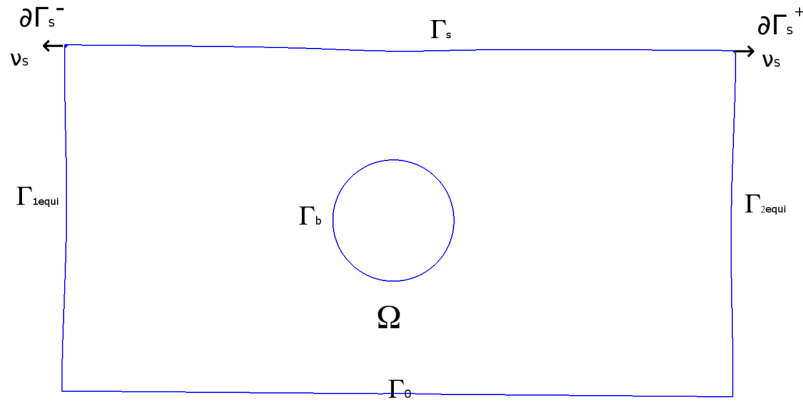


**Figure 3.** Calculated geometry of the new computational domain in the case of a solid body size large compared to initial computational domain. The digging effect on  $\Gamma_s$  and the inwards bowing of  $\Gamma_{1equi}$  and  $\Gamma_{2equi}$  are more pronounced than in our case.

### 3.2.2. Transient state

We study the evolution of a small disturbance around the steady state  $(\rho_0, \varphi_0, \eta_0)$ . The unsteady waves in the fluid are represented by the perturbation functions  $\rho, \varphi, \eta$  of variables  $x(x_1, x_2)$  and  $t$ . The problem is formulated with them wherein  $\rho_{tot}(x, t) = \rho_0(x) + \rho(x, t)$ ,  $\Phi(x, t) = U\varphi_0(x) + \varphi(x, t)$ ,  $\eta_{tot}(x, t) = \eta_0(x) + \eta(x, t)$ . The solution is split into main background steady state component and a transient one. The domain  $\Omega$  is then cropped by  $\Gamma_0, \Gamma_b, \Gamma_s = \eta_0, \Gamma_{1equi}$  and  $\Gamma_{2equi}$  as shown in figure 3. The new lateral boundaries  $\Gamma_{1equi}$  and  $\Gamma_{2equi}$  correspond to equipotential lines of  $\varphi_0$  passing respectively through left upper domain corner and right upper corner of  $\Omega$ . As result, the main steady flow crosses perpendicularly  $\Gamma_{1equi}$  and  $\Gamma_{2equi}$  and no tangential flow remains in the new domain  $\Omega$ . The artificial boundaries are chosen far enough from rigid body to consider that steady state flow is uniform in this area and so the corners of the new domain are right-angled. The disturbance is so small that it is then reasonable to neglect the non-linear terms in the governing equations Eq.(5)-Eq.(8) to obtain Eq.(11)-Eq.(14). Convective derivatives with flow velocity  $U\nabla\varphi_0$  are used to derive linearized equations Eq.(12) and Eq.(13). Hence  $(\rho, \varphi, \eta)$  are assured to satisfy the linearized enhanced Neumann-Kelvin's model with capillarity :

- The linearized continuity equation

$$\frac{\partial \rho}{\partial t} + U\nabla\rho \cdot \nabla\varphi_0 + \rho_0\Delta\varphi = 0 \quad \text{in } \Omega \times ]0, T[. \quad (11)$$

- The linearized momentum equation for the inner fluid

$$\frac{\partial^2 \varphi}{\partial t^2} + 2U\nabla\varphi_0 \cdot \nabla \left( \frac{\partial \varphi}{\partial t} \right) + U^2\nabla\varphi_0 \cdot \nabla(\nabla\varphi_0 \cdot \nabla\varphi) - c_f^2\Delta\varphi = 0 \quad \text{in } \Omega \times ]0, T[ \quad (12)$$

$$\text{given that } \frac{1}{2}|\nabla\varphi_0|^2 + \nabla F(\rho_0) = 0 \quad \text{and} \quad \frac{\partial F(\rho_0)}{\partial \rho_{tot}} = \frac{c_f^2}{\rho_0}.$$

- The linearized momentum equation for the surface fluid

$$2\varepsilon\rho_0\left(\frac{\partial^2\eta}{\partial t^2}+2U\nabla_s\varphi_0\cdot\nabla_s\left(\frac{\partial\eta}{\partial t}\right)+U^2\nabla_s\varphi_0\cdot\nabla_s(\nabla_s\varphi_0\cdot\nabla_s\eta)\right) = \sigma\Delta_s\eta - \rho_0g\eta - \rho_0\frac{\partial\varphi}{\partial t} - \rho_0U\nabla_s\varphi_0\cdot\nabla_s\varphi \quad \text{in } \Gamma_s\times]0, T[ \quad (13)$$

where  $\cdot$  denotes the scalar product. Since the domain of study was reshaped,  $\nabla_s\eta_0$  and  $\Delta_s\eta_0$  are set to zero on  $\Gamma_s$ .

- The continuity of normal velocity at the interface

$$\frac{\partial\varphi}{\partial\nu} = \frac{\partial\eta}{\partial t} + U\nabla_s\varphi_0\cdot\nabla_s\eta \quad \text{in } \Gamma_s\times]0, T[. \quad (14)$$

- The non-penetrability condition leads to homogeneous Neumann boundary condition for  $\varphi$

$$\frac{\partial\varphi}{\partial\nu} = 0 \quad \text{in } \Gamma_0\cup\Gamma_b\times]0, T[. \quad (15)$$

- The initial condition corresponding to a disturbance taking place in the fluid: the functions  $\varphi(x, 0)$  and  $\partial\varphi/\partial t(x, 0)$  are set as Gaussian pulse functions in  $\Omega$  and the functions  $\eta(x, 0)$  and  $\partial\eta/\partial t(x, 0)$  are fixed to zero on  $\Gamma_s$ .

### 3.2.3. Lateral artificial boundary conditions

Non-reflecting boundary condition applied on inner fluid lateral edges is :

$$a\frac{\partial\varphi}{\partial t} + \left(U\frac{\partial\varphi_0}{\partial\nu} + c_f\right)\frac{\partial\varphi}{\partial\nu} = 0 \quad \text{in } \Gamma_{1equi}\cup\Gamma_{2equi}\times]0, T[ \quad (16)$$

where  $c_f$  denotes the speed of sound in the fluid and  $a$  a parameter related to the angle of incidence waves with respect to the normal of the boundary surface. This relation is consistent with Sommerfeld-like or zero order non reflecting boundary condition for a wave which propagates at the phase velocity  $c_f$  corrected by the normal to the boundary component of velocity of the main background steady flow  $U\partial\varphi_0/\partial\nu$ . In the following the parameter  $a$  is set to 1, this implies that the angles of incidence of impinging disturbances are close to the normal of the boundary. For such an order of approximation of absorbing boundary condition, it is not beneficial to set  $a \neq 1$  [23]. On the surface bounds  $\partial\Gamma_s$  non-reflecting conditions imposed is the natural Sommerfeld-like non reflecting boundary condition,

$$\frac{\partial\eta}{\partial t} + \left(U\frac{\partial\varphi_0}{\partial\nu_s} + c_r\right)\frac{\partial\eta}{\partial\nu_s} = 0 \quad \text{in } \partial\Gamma_s \quad \forall t \in ]0, T[ \quad (17)$$

where  $c_r$  denotes the riddle velocity with  $c_r^2 = \sigma/2\rho_0\varepsilon$  derived from Eq.(13). It is consistent with the one dimensional zero order non-reflecting boundary condition for a propagating wave at velocity  $c_r$  in an uniform background steady flow of velocity  $U\partial\varphi_0/\partial\nu_s$ . This boundary condition introduces a mathematical specific damping on each boundary nodes of the surface  $\Gamma_s$  in order to attenuate spurious reflecting modes.

## 4. Solution method

A classical approach for addressing waves propagation in layered media with a wave source close to interfaces is first to look for a solution as a superposition of plane harmonic waves i.e. applying Laplace transform in time and Fourier transform in space to the problem. Dispersion relation, phase and group velocities and others significant quantities are thus derived to characterize



waves propagation properties in the stratified structure. But in our case, due to the complexity of the coupled equations involved, a weak form of the problem and thereafter a finite element formulation are directly considered to obtain the solution.

#### 4.1. Variational formulation and numerical approach

Multiplying Eq.(12) by  $\psi \in H^1(\Omega)$  and Eq.(13) by  $v \in H^1(\Gamma_s)$  respectively together with Green's formula application lead to the following coupled variational formulation :

Find functions  $(\varphi, \eta) \in H^1(\Omega) \times H^1(\Gamma_s) \times L^2(]0, T[)$  such that  $\forall(\psi, v) \in H^1(\Omega) \times H^1(\Gamma_s)$

$$\begin{aligned} & \int_{\Omega} \dot{\varphi} \psi d\tau + U \int_{\Omega} \nabla \varphi_0 \cdot (\nabla \dot{\varphi} \psi - \dot{\varphi} \nabla \psi) d\tau + c_f \int_{\Gamma} \dot{\varphi} \psi d\tau + c_f^2 \int_{\Omega} \nabla \varphi \cdot \nabla \psi d\tau \\ & - U^2 c_f^2 \int_{\Omega} (\nabla \varphi_0 \cdot \nabla \varphi) (\nabla \varphi_0 \cdot \nabla \psi) d\tau - c_f^2 \int_{\Gamma_s} \dot{\eta} \psi d\tau - U c_f^2 \int_{\Gamma_s} \nabla_s \varphi_0 \cdot \nabla_s \eta \psi d\tau = 0 \end{aligned} \quad (18)$$

and

$$\begin{aligned} & 2\varepsilon c_f^2 \int_{\Gamma_s} (\dot{\eta} v + U \nabla_s \varphi_0 (\nabla_s \dot{\eta} v - \dot{\eta} \nabla_s v) - U^2 (\nabla_s \varphi_0 \cdot \nabla_s \eta) (\nabla_s \varphi_0 \cdot \nabla_s v)) d\sigma \\ & - 2\varepsilon c_f^2 U \int_{\Gamma_s} (U v \Delta_s \varphi_0 (\nabla_s \varphi_0 \cdot \nabla_s \eta) + v \Delta_s \varphi_0 \dot{\eta}) d\sigma + \frac{c_f^2}{\rho_0} \int_{\Gamma_s} \sigma \nabla_s \eta \cdot \nabla_s v d\sigma \\ & + \frac{c_f^2}{\rho_0} \int_{\Gamma_s} \rho_0 \eta g v d\sigma + c_f^2 \int_{\Gamma_s} \dot{\varphi} v d\sigma - c_f^2 U \int_{\Gamma_s} \nabla_s \varphi_0 \cdot \nabla_s v \varphi + v \Delta_s \varphi_0 \varphi d\sigma \\ & + \left[ c_f^2 U \frac{\partial \varphi_0}{\partial \nu_s} \varphi v + 2\varepsilon c_f^2 c_r \dot{\eta} v \right]_{\partial \Gamma_s} = 0. \end{aligned} \quad (19)$$

Physical field approximation is performed by classical finite element method. A finite dimension subspace  $V_h \subset H^1(\overline{\Omega})$  made of piecewise linear functions on a fixed mesh, characterized by element length  $h$ , is considered. Letting  $V_h = \text{span}(\varphi_1, \varphi_2, \dots, \varphi_{N1}, \eta_1, \eta_2, \dots, \eta_{N2})$  with  $\varphi_{i \ 1 \leq i \leq N1}$  and  $\eta_{i \ 1 \leq i \leq N2}$  finite element shape functions on  $\Omega$  and on  $\Gamma_s$  respectively. Calling  $X$  the coordinate vector of  $\mathcal{X}(\varphi, \eta)$  relative to this basis leads to the recasted algebraic differential linear problem :

Find  $X(t) \in R^N$ ,  $N = N1 + N2$ ,  $t \in ]0, T[$  such that

$$M\ddot{X} + C\dot{X} + KX = 0 \quad (20)$$

with  $X(0), \dot{X}(0)$  prescribed.  $M, C, K$  are sparses matrices. Centered finite difference schemes are applied for the time domain approximation in order to avoid numerical instabilities. Finally the problem becomes :

Find  $X^{(n)} \in R^N$ ,  $n > 1$ , such that

$$A_1 X^{(n+1)} = A_2 X^{(n)} + A_3 X^{(n-1)} \quad (21)$$

where  $A_1, A_2$  et  $A_3$  are sparse matrices depending on  $M, C, K$  and  $\Delta t$  with  $\Delta t$  the time step chosen.

The computing process is fully automated. All the geometry operations and meshes are generated and updated automatically according intermediate results by a batch program using Numpy and Scipy Python routines and GMSH [35]. Due to the complexity of weak formulation

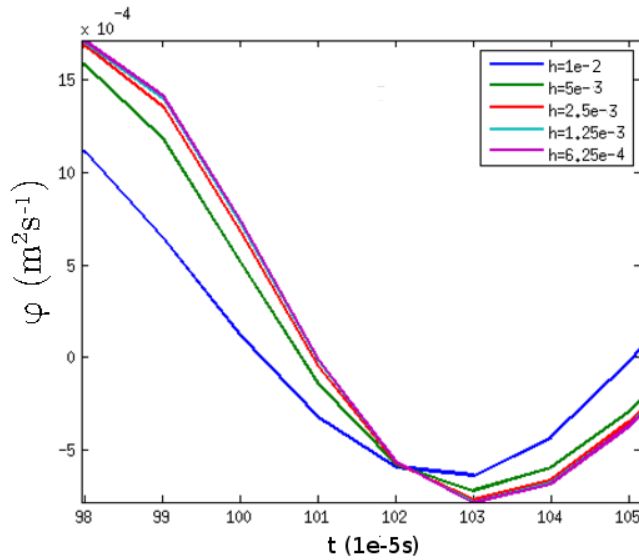


**Figure 4.** Inner fluid velocity potential  $\varphi$  ( $\text{m}^2\text{s}^{-1}$ ) at point of coordinates (0.5,0.5) versus time ( $10^{-5}\text{s}$ ) for different elements sizes of the mesh.

terms, low-level generic assembly procedures of GETFEM++ is employed to make the assembly of the involved sparse matrices in Eq.(20) [36]. To compute the solution of the large sparse system Eq.(21) a parallel sparse direct solver (MUMPS) is used. For the post processing handling, Matplotlib Python libraries, PARAVIEW and GMSH are utilized [37]. Mesh convergence study is performed by reducing characteristic size of elements,  $h$ , from  $h = 10^{-2}$  to  $h = 6.25 \times 10^{-4}$ . As shown in figures 4 and 5, results converge upon the same solution as the mesh density increases. A satisfactory compromise between accuracy of results and computing time can be achieved by choosing the value of  $h = 1.25 \times 10^{-3}$ . This result is consistent with the order of magnitude of the wavelength of gravity-capillary waves of interest ( $\lambda \approx 10^{-2}\text{m}$ ). Indeed the solution is curvy or even oscillates over the wavelength this means to use sufficient fine meshes or high order piecewise polynomials to get a reliable approximation by finite element method. A classic rule to reduce interpolation errors is to set the resolution of the wave  $n_{res} = \lambda/h \approx 10$  (here  $h/\lambda = 8$ ) for linear piecewise polynomial but at small wavelength it appears to be insufficient due to a numerical pollution identified in Helmholtz problems [38, 39]. For numerical computations, values of parameters of table 4.1 are used. The value of  $H$  is set to ensure that surface waves progress over deep water. The value of  $U$  is chosen to be less than  $\sqrt[4]{4g\sigma/\rho_0} \approx 0.23 \text{ m}\cdot\text{s}^{-1}$  so that the flow becomes an uniform stream with constant velocity  $U$  at infinity [33].

Parameters	$L(\text{m})$	$H(\text{m})$	$R(\text{m})$	$U(\text{m}\cdot\text{s}^{-1})$	$\varepsilon(\text{m})$	$\sigma(\text{N}\cdot\text{m}^{-1})$
Values	1	1	$5\cdot 10^{-2}$	0.15	$10^{-3}$	0.075

**Table 1.** Numerical computational values of parameters of the problem.

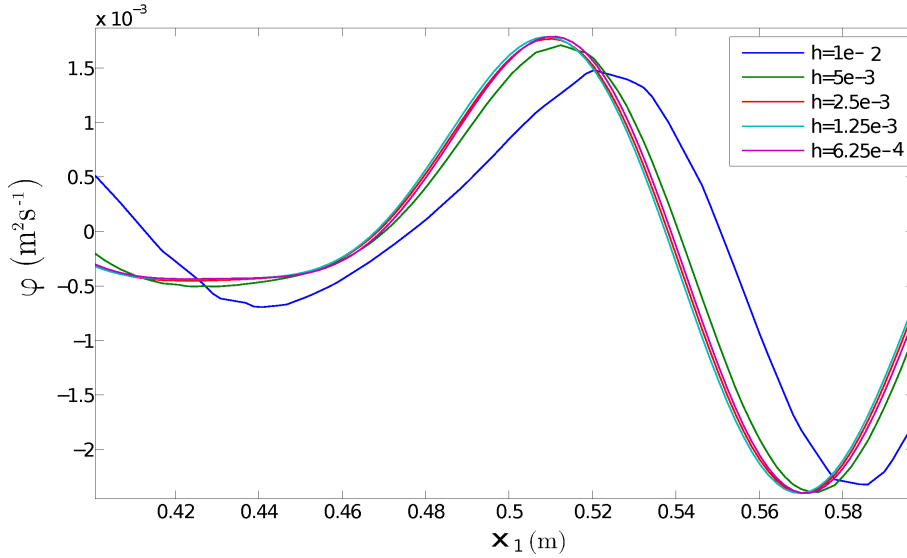


**Figure 5.** Inner fluid velocity potential  $\varphi$  ( $\text{m}^2\text{s}^{-1}$ ) for different mesh densities along a part of the middle line of computational domain (m) at  $t = 100\Delta t_\nu$ .

## 5. Results and comments

Wave propagation phenomenon is monitored by the variation of  $\varphi$  in the inner fluid and the variation of  $\eta$  on the surface respectively. The value of time step chosen is  $\Delta t_\nu = 10^{-5}\text{s}$  in order to see properly wave propagation with a velocity of  $c_f$  across the extend of the computational domain  $\Omega$ . As it can be seen on figure 6, reflecting waves appear on the bottom of the domain as on the surface of the immersed solid body where homogeneous Neumann conditions are imposed to model non penetrability of the fluid through them. In addition, on both lateral sides of the computational domain no spurious reflecting wave appears to be present. Thanks to hyperbolicity of the problem, in order to verify whether non-reflecting boundary conditions are satisfactory on inner fluid lateral edges Eq.(16), a similar study is carried out according to the same previous calculation criteria on a larger computational domain in  $x_1$  direction, sized so as to avoid lateral side spurious reflecting waves during the all simulation time [23]. The new solution obtained is regarded as a reference solution. Both resulting waves are in phase but a variable amplitude difference can be noticed. The wave is slightly reflected especially on its peak of amplitude for times when there are not many interference. Indeed absorbing boundary conditions chosen are not intended to handle such a situation (see figure 7).

Waves propagation in inner fluid results in deformation of the surface as shown in figures 8 and 9. The corresponding normal displacement  $\eta$  propagates along the surface  $\Gamma_s$ . On each side of the surface,  $\partial\Gamma_s$ , no spurious reflective wave is noticed. In inner fluid layer no wave related with any reflective surface on surface is neither observed (see figure 9). Then lateral boundary conditions introduced by Eq.(17) seem to be also adequate to successfully model the propagating phenomenon on the surface. Nevertheless the velocity of the phenomenon is the same as in inner fluid layer which is not in complete agreement with surface layer material properties and wave propagation in stratified media theories [11, 13]. The expected value should be closed to the riddle velocity  $c_r$ . Therefore no surface propagation phenomenon should be observed with time

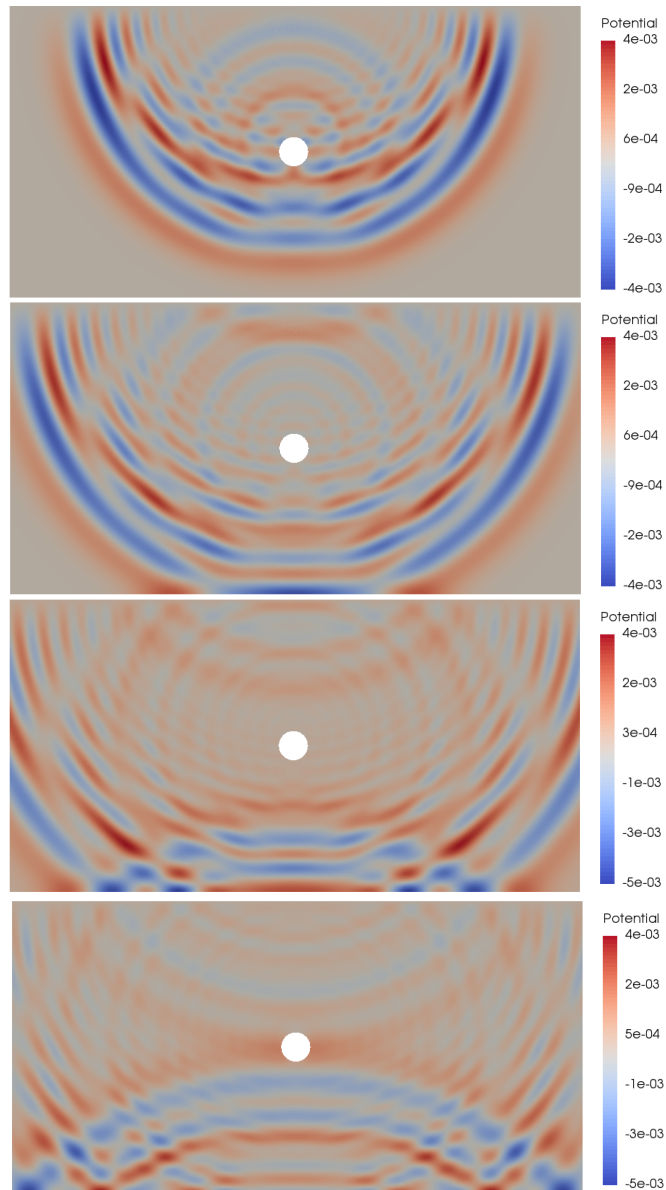


**Figure 6.** Propagation of velocity potential disturbance  $\varphi$  at times:  $t = 80\Delta t_v$ ,  $t = 100\Delta t_v$ ,  $t = 120\Delta t_v$ ,  $t = 140\Delta t_v$ . The order of magnitude of initial perturbation is  $10^{-2}\text{m}^2\text{s}^{-1}$ .

step  $\Delta t_v$ . That's actually what happens when initial disturbance is located just below or on the surface as shown in figure 10. The observed normal displacements  $\eta$  in figures 8 and 9 are not related directly to surface wave propagation, but rather primarily to the velocity potential acoustic wave propagation in inner fluid layer and to the interface coupling between the potential  $\varphi$  and the normal displacement  $\eta$  on  $\Gamma_s$  given by Eq.(14). The energy transmitted to the surface layer by the inner layer remains stationary over the time range considered. Therefore application of lateral boundary conditions Eq.(17) does not significantly affect the propagation phenomenon and its accuracy can not be estimated with an initial perturbation in inner fluid layer.

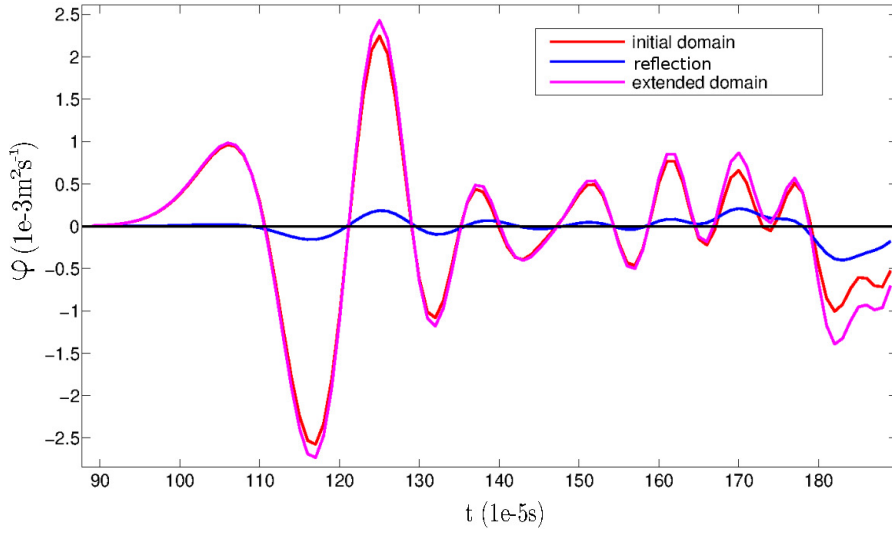


**Figure 7.** Comparison of inner fluid velocity potentials  $\varphi$  ( $10^{-3}\text{m}^2\text{s}^{-1}$ ) versus time ( $10^{-5}\text{s}$ ) between extended and main computational domain on the middle of right artificial lateral edge.

Numerical simulations are then carried out in the case of an initial disturbance of the surface with a time step  $\Delta t_s = 10^{-2}\text{s}$ . The functions  $\varphi(x, 0)$  and  $\partial\varphi/\partial t(x, 0)$  are set to zero in  $\Omega$  and  $\eta(x, 0)$  and  $\partial\eta/\partial t(x, 0)$  are introduced as Gaussian pulse functions on  $\Gamma_s$ . Surface waves propagate along  $\Gamma_s$  (see figures 10 and 11) but singularities appear on each side of the surface  $\partial\Gamma_s$  as shown on figure 12. In fact due to the significant difference between the wave propagation characteristic velocity values of the surface and inner fluid layers, singularities come out on the intersection between the artificially chosen boundaries of the domain and the two layers' interface when Sommerfeld non reflecting boundary conditions are applied. The non reflecting boundary condition on the lateral edges Eq.(13) has to be changed to handle these difficulties [40]. To this end, as the conditions are to be set for the points  $\partial\Gamma_s$  that belong to the surface  $\Gamma_s$  and to the lateral boundaries  $\Gamma_{1equi}$  or  $\Gamma_{2equi}$ , the equations Eq.(13), Eq.(14) and Eq.(16) are considered to devise the new boundary conditions. The guiding idea is to extend the non reflective boundary condition applied on the lateral boundaries  $\Gamma_{1equi}$  or  $\Gamma_{2equi}$  Eq.(16) to the surface  $\Gamma_s$  intersecting points  $\partial\Gamma_s$  Eq.(13) by means of the normal velocity continuity condition Eq.(14). Using the simplifying assumptions  $\varphi_0 = x_1$ ,  $s = x_1$  and  $(v_s \cdot e_1) = \pm 1$  led by choosing  $\Gamma_{1equi}$  and  $\Gamma_{2equi}$  away from rigid body, the following simplified equations must be satisfied on  $\partial\Gamma_s$  :

$$\frac{\partial^2 \eta}{\partial t^2} + 2U \frac{\partial^2 \eta}{\partial x_1 \partial t} + (U^2 - c_r^2) \frac{\partial^2 \eta}{\partial x_1^2} + \frac{1}{2\varepsilon} \left( \frac{\partial \varphi}{\partial t} + U \frac{\partial \varphi}{\partial x_1} \right) + \frac{g}{2\varepsilon} \eta = 0, \quad (22)$$

$$\frac{\partial \varphi}{\partial x_2} = \frac{\partial \eta}{\partial t} + U \frac{\partial \eta}{\partial x_1}, \quad (23)$$

$$\frac{\partial \varphi}{\partial t} + (U + c_f) \frac{\partial \varphi}{\partial x_1} = 0 \quad \text{on } \Gamma_s \cap \Gamma_{2equi}, \quad (24)$$

$$\frac{\partial \varphi}{\partial t} + (U - c_f) \frac{\partial \varphi}{\partial x_1} = 0 \quad \text{on } \Gamma_s \cap \Gamma_{1equi}. \quad (25)$$

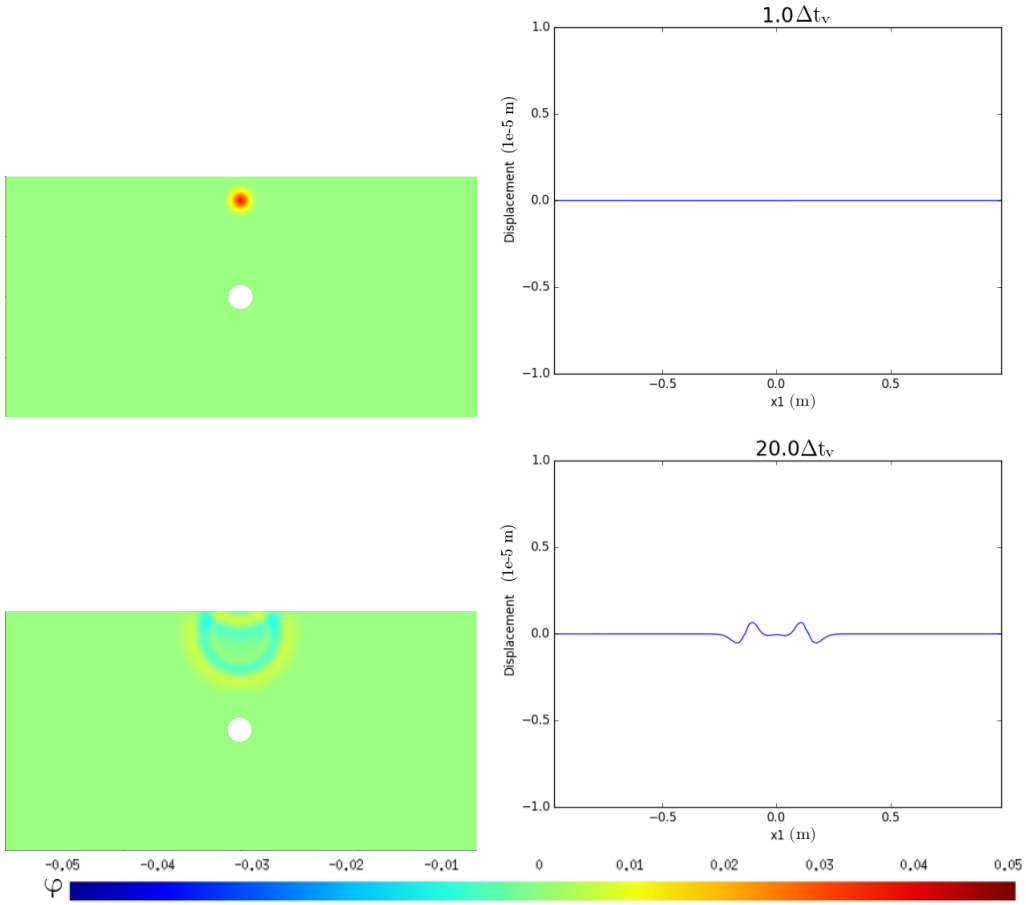


**Figure 8.** Propagation of disturbance  $\varphi$  in  $\Omega$  and related normal surface displacement  $\eta$  ( $10^{-5}\text{m}$ ) on  $\Gamma_s$  versus  $x_1$  coordinate (m) at times:  $t = \Delta t_v$ ,  $t = 20\Delta t_v$ . The initial order of magnitude of  $\varphi$  is  $10^{-2}\text{m}^2\text{s}^{-1}$ . Its propagating order of magnitude is  $10^{-3}\text{m}^2\text{s}^{-1}$  and the order of magnitude of the normal displacement is  $10^{-6}\text{m}$ .

For the right side (resp. the left side), the solution method consists in derivating first Eq.(24) (resp. Eq.(25)) with respect to  $x_2$  and Eq.(23) with respect to  $x_1$  and  $t$ , in order to eliminate partial derivatives of  $\varphi$ . Introducing the resulting expression into Eq.(22) leads, after integrating with respect to time, to the following new boundary condition in cartesian coordinates for each edge,

$$Z^\pm \frac{\partial \eta}{\partial t} + A^\pm \frac{\partial \eta}{\partial x_1} + B^\pm \int_0^t \eta ds + C^\pm \varphi = 0 \quad \text{on } \partial\Gamma_s^\pm \quad (26)$$

with  $A^\pm, B^\pm, C^\pm, Z^\pm$  depending on  $U, c_f, c_r, \epsilon, g$ . The symbol  $-$  denotes that condition is on the left boundary of  $\Gamma_s$  and  $+$  on the right one. The boundary conditions obtained are said non local in time as they depend not only on the time  $t$  but also on entire history of  $\eta$  on  $\partial\Gamma_s$ . The second part of variational formulation Eq.(19) becomes within the new non reflective boundary conditions Eq.(26):

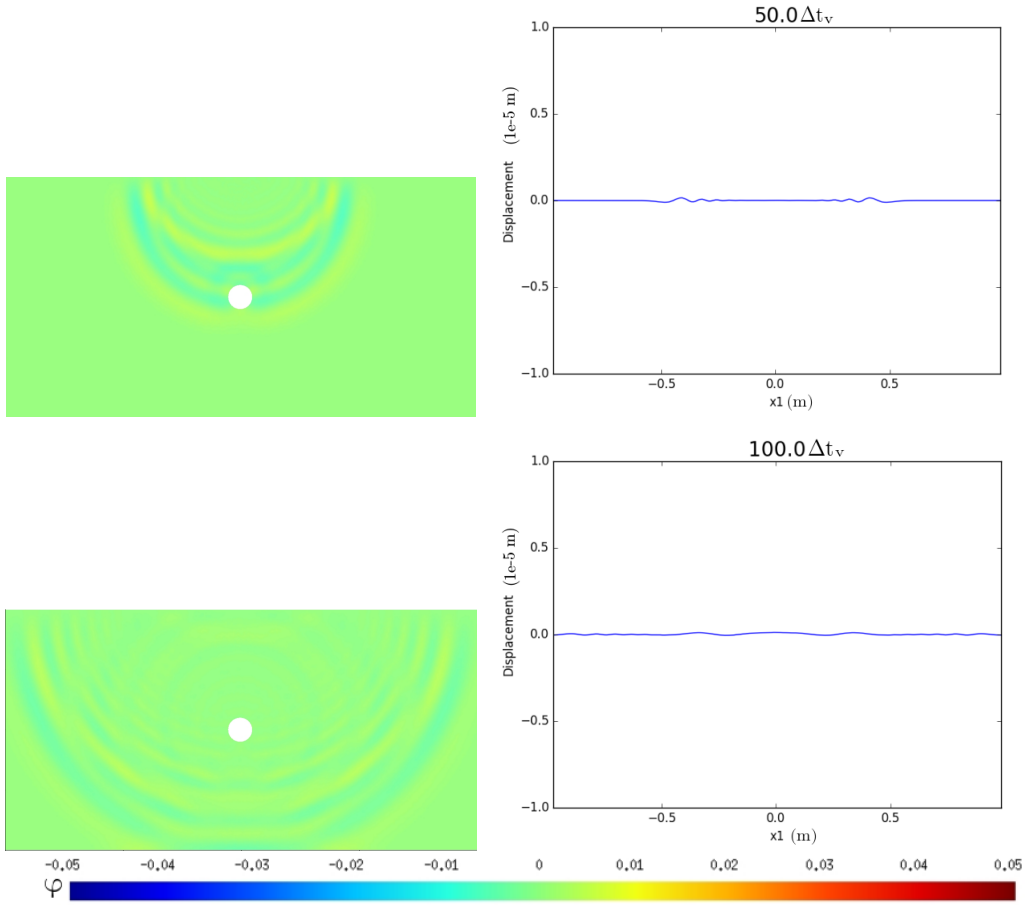


**Figure 9.** Propagation of disturbance  $\varphi$  in  $\Omega$  and related normal surface displacement  $\eta$  ( $10^{-5}\text{m}$ ) on  $\Gamma_s$  versus  $x_1(m)$  coordinate at times:  $t = 50\Delta t_v$ ,  $t = 100\Delta t_v$ . Its order of magnitude is  $10^{-3}\text{m}^2\text{s}^{-1}$  and corresponding normal displacement  $\eta$  order of magnitude is  $10^{-6}\text{m}$ .

$$\begin{aligned}
& 2\epsilon c_f^2 \int_{\Gamma_s} (\ddot{\eta}v + U\nabla_s\varphi_0(\nabla_s\dot{\eta}v - \dot{\eta}\nabla_s v) - U^2(\nabla_s\varphi_0 \cdot \nabla_s\eta)(\nabla_s\varphi_0 \cdot \nabla_s v)) d\sigma \\
& - 2\epsilon c_f^2 U \int_{\Gamma_s} (Uv\Delta_s\varphi_0(\nabla_s\varphi_0 \cdot \nabla_s\eta) + v\Delta_s\varphi_0\dot{\eta}) d\sigma + \frac{c_f^2}{\rho_0} \int_{\Gamma_s} \sigma\nabla_s\eta \cdot \nabla_s v d\sigma \\
& + \frac{c_f^2}{\rho_0} \int_{\Gamma_s} \rho_0\eta g v d\sigma + c_f^2 \int_{\Gamma_s} \dot{\varphi} v d\sigma - c_f^2 U \int_{\Gamma_s} \nabla_s\varphi_0 \cdot \nabla_s v \varphi + v\Delta_s\varphi_0\varphi d\sigma \\
& + \left[ \left( E^\pm \dot{\eta} + F^\pm \int_0^t \eta ds + G^\pm \varphi \right) v \right]_{\partial\Gamma_s} = 0.
\end{aligned} \tag{27}$$

with  $E^\pm, F^\pm, G^\pm$  depending on  $U, c_f, c_r, \epsilon, g$ . The previous solution method is used to solve the new variational problem Eq.(18) and Eq.(27). For the time domain approximation, centered

finite difference scheme is applied for derivatives and trapezoidal rule is used for the integral over time term. The problem becomes finding  $X^{(n)} \in R^N$ ,  $n > 1$ , such that

$$A_1 X^{(n+1)} = A_2 X^{(n)} + A_3 X^{(n-1)} + F \quad (28)$$

where  $A_1$ ,  $A_2$  et  $A_3$  are sparse matrices depending on  $M$ ,  $C$ ,  $K$  and  $\Delta t$ ;  $F$  a vector depending on  $F^\pm$  and  $\Delta t$  accounting for non local condition term in time Eq.(26) with non zero component corresponding to the surface edges  $\partial\Gamma_s$ .

A numerical simulation is carried out with an initial surface excitation and a time step  $\Delta t_s$ . Singularities seem to be no longer present on  $\partial\Gamma_s$  and waves can get out of computational domain without generating significant spurious reflections (see figure 13). Comparison between the old and the new non reflective boundary condition results is done over two thousand time steps  $\Delta t_s$  to check any singularities (see figure 15). Similarly to the previous case to verify non-reflecting boundary conditions on surface edges Eq.(26), a larger computational domain in  $x_1$  direction is chosen to compute a reference solution. Both resulting waves are in phase but a varying amplitude difference can be noticed due to existing spurious reflections (see figure 14) which fade away over time (see figure 13). According to the ratio between the orders of magnitude of the inner fluid potential and the surface displacement noticed in each calculated cases, it comes out that the inner fluid wave propagation effect is not significant in the case of initial disturbance nearby the surface or on the surface itself. Indeed, a velocity potential of order of magnitude of  $10^{-3} \text{m}^2 \text{s}^{-1}$  on the surface leads to a normal displacement response of order of magnitude of  $10^{-6} \text{m}$  in inner fluid initial perturbation case. But in surface initial disturbance case where the order of magnitude of normal displacement is  $10^{-6} \text{m}$ , the velocity potential barely reaches  $10^{-6} \text{m}^2 \text{s}^{-1}$  on the surface, the linearity of the model leads to a normal displacement response of  $10^{-9} \text{m}$ , therefore negligible compared to  $10^{-6} \text{m}$  (see figures 8, 9, 10 and 11). Thus the waves propagate mainly in the surface layer guided in the medium of smaller velocity in totally agreement with wave propagation theories in stratified media. Actually, during surface wave propagation, a small amount of energy is steadily transferred from the surface to inner fluid which is immediately removed from the computational domain as in an incompressible fluid. The velocity potential  $\varphi$  rendering (see figure 11) comes from the superposition of all velocity potential waves generated by the propagating surface wave at all times. Therefore these results can hardly be analyzed and used to clearly draw any possible conclusions on the compliance of the non reflecting boundary condition chosen Eq.(16) in inner fluid layer.

## 6. Conclusion

For the modelling of the wake of a solid body moving through a body of water, a wave propagation problem in a convective stratified media has been considered. To numerically solve the problem, the finite elements method is applied due to its versatility and its results accuracy in dealing with complex configurations. Nevertheless since it is an acoustic scattering problem with large wavenumber waves which is of interest, a fine mesh in artificially bounded domain has to be used and appropriate non-reflecting boundary conditions are to be sought while keeping computational costs low. In addition, the significant differences between layer properties make difficult to address the entire problem with traditional schemes, a non local in time boundary condition has been devised by taking into account all the conditions that must be met on the artificial lateral edges of the computational domain. This work has highlighted complex phenomena that involve the coupled propagation of surface and volume waves at different time scales and with very different orders of magnitude, features that cannot be observed under the assumption of fluid incompressibility. To go further with the same model, it is necessary to reduce



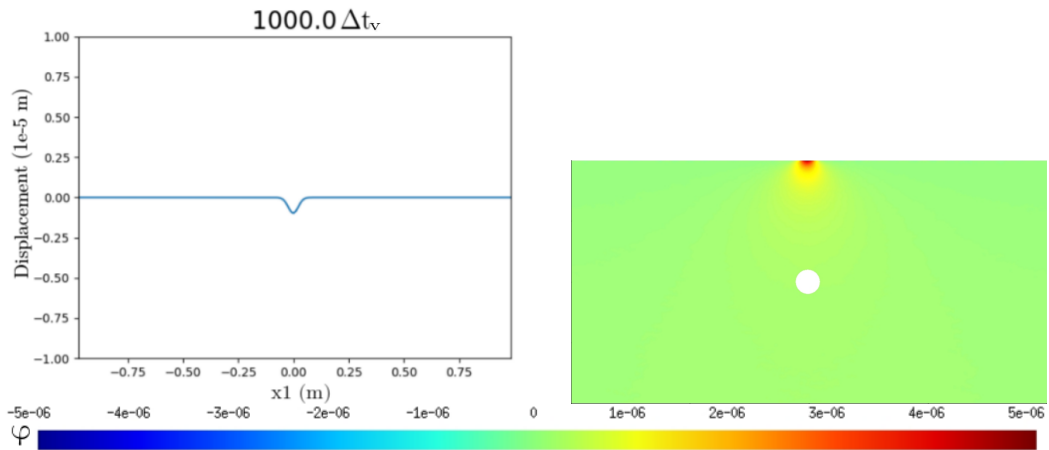


**Figure 10.** Propagation of normal surface displacement  $\eta$  on  $\Gamma_s$  versus  $x_1$  coordinate and related disturbance  $\varphi$  in  $\Omega$  at time  $t = 1000\Delta t_v = \Delta t_s$ . Initial perturbation is located on the surface of the fluid. The order of magnitude of  $\eta$  is  $10^{-6}$ m. The order of magnitude of the potential  $\varphi$  transmitted to the surface of inner fluid is  $10^{-6}\text{m}^2\text{s}^{-1}$ .

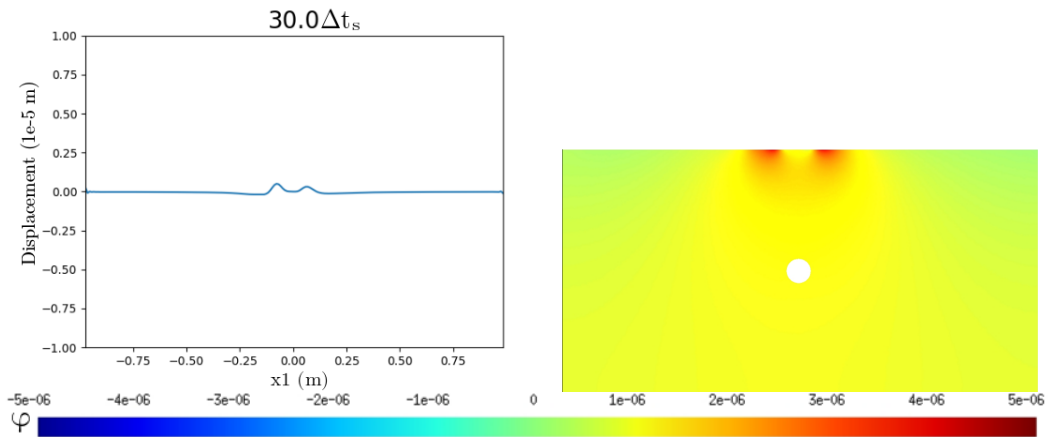


**Figure 11.** Propagation of normal surface displacement  $\eta$  on  $\Gamma_s$  versus  $x_1$  coordinate and related disturbance  $\varphi$  in  $\Omega$  at time  $t = 30\Delta t_s$ . Initial disturbance is located on the surface of the fluid. Order of magnitude of propagating  $\eta$  is  $10^{-6}$ m. The order of magnitude of the potential  $\varphi$  transmitted to the surface of inner fluid is  $10^{-6}\text{m}^2\text{s}^{-1}$ .

the size of the linear system by using suitable enriched basis functions [41,42] in order to decrease the number of elements per wavelength and to be able to increase the order of the absorbing boundary condition to eliminate spurious reflections. Due to the differences in scale between the phenomena occurring in each layer and the weak feedback from the inner fluid to the surface, a more simple one-dimensional model could be also considered by adding a damping term to model the energy dissipation of the surface propagating wave into the fluid.

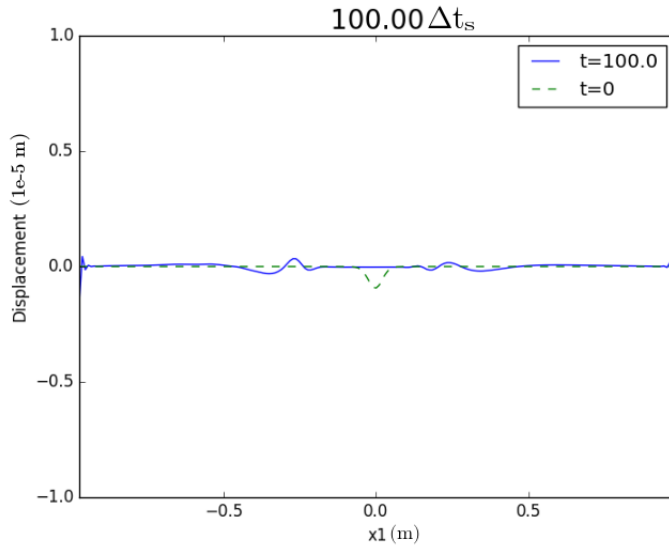


**Figure 12.** Displacement  $\eta$  ( $10^{-5}m$ ) of the surface  $\Gamma_s$  at time  $t = 100\Delta t_s$  versus  $x_1$  coordinate ( $m$ ). Initial disturbance is located on the surface  $\Gamma_s$  in dash point. Singularities appear on the edges of the surface  $\partial\Gamma_s$ .

### Acknowledgment

I would like to thank Professor Philippe Destuynder, at University of La Rochelle (Laboratory LaSIE), for fruitful discussions.

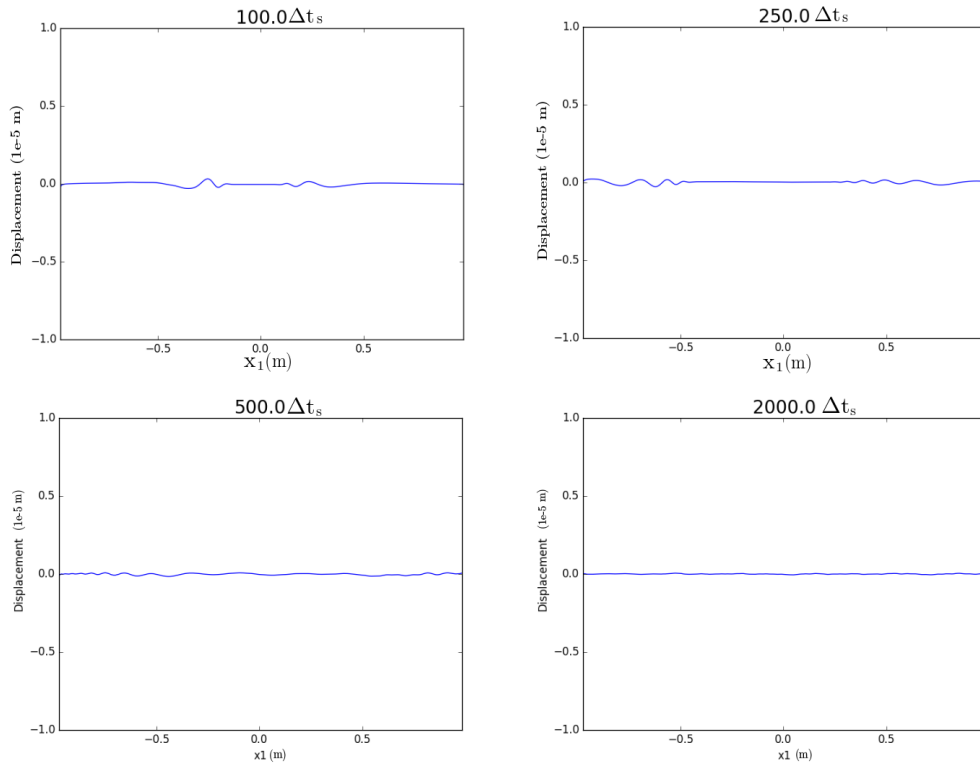


**Figure 13.** Displacement  $\eta(10^{-5} m)$  of the surface  $\Gamma_s$  versus  $x_1$  coordinate ( $m$ ) at:  $t = 100\Delta t_s$ ,  $t = 250\Delta t_s$ ,  $t = 500\Delta t_s$  and  $t = 2000\Delta t_s$ . Initial disturbance is located on the surface  $\Gamma_s$ . The waves propagate without any singularity on surface edges but spurious reflections on surface are still present

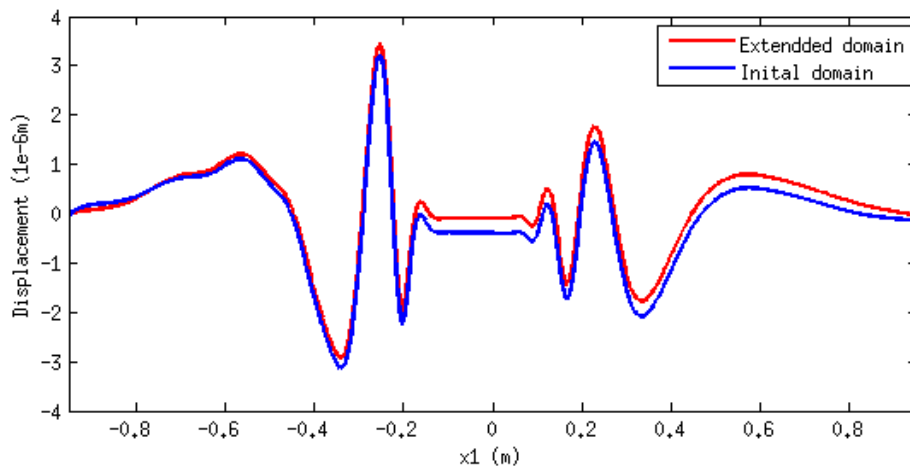


**Figure 14.** Comparison between normal displacements  $\eta(10^{-6} m)$  of surface  $\Gamma_s$  in initial and extended domain cases versus  $x_1(m)$  at  $t = 100\Delta t_s$ .

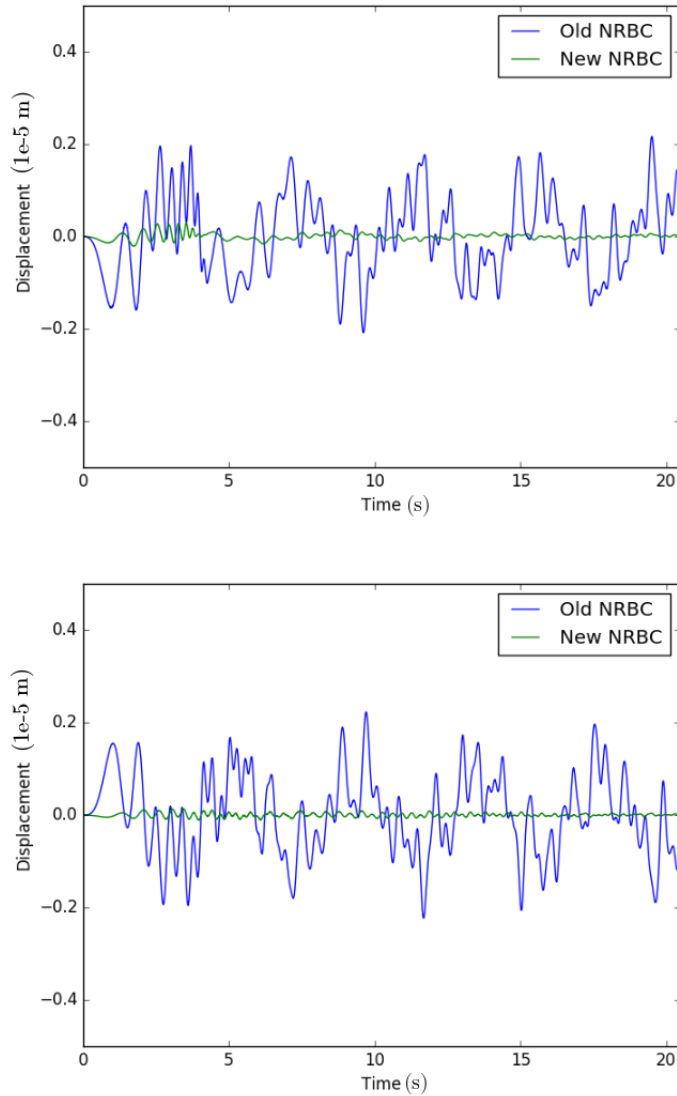


**Figure 15.** Comparison of the results for displacement  $\eta(10^{-5}m)$  at  $\partial\Gamma_s^-$  and at  $\partial\Gamma^+$  obtained by the two non reflective boundary conditions (NRBC) and over simulation time  $2000\Delta t_s$ .

## References

- [1] G. B. Airy, *Tides and waves*, B. Fellowes, 1845.
- [2] G. G. Stokes, "On the theory of oscillatory waves", *Transactions of the Cambridge philosophical society* (1880).
- [3] J. Lighthill, *Waves in fluids*, Cambridge university press, 2001.
- [4] M. S. Longuet-Higgins, "Eulerian and Lagrangian aspects of surface waves", *Journal of Fluid Mechanics* **173** (1986), p. 683–707.
- [5] J. W. Miles, "On the generation of surface waves by shear flows", *Journal of Fluid Mechanics* **3** (1957), no. 02, p. 185–204.
- [6] J. Stocker, "Water waves", *Pure and Applied Mathematics* **9** (1957), p. 291–314.

- [7] G. B. Whitham, *Linear and nonlinear waves*, vol. 42, John Wiley & Sons, 2011.
- [8] M. Bauer, "Le problème de Neumann-Kelvin", *Annali di Matematica Pura ed Applicata* **124** (1980), no. 1, p. 233-255.
- [9] A. Cariou, "Une méthode de calcul par éléments finis de la résistance de vague des corps flottants ou immergés en théorie linéaire", *Revue de l'Institut Français du Pétrole* **33** (1978), no. 1, p. 59-82.
- [10] P. Guével, G. Delhommeau, D. Euvrard, S. Marcouyoux, "Résistance d'ondes d'un navire de surface", *La Houille Blanche* **1977** (1977), no. 5-6, p. 429-439.
- [11] L. Brekhovskikh, *Waves in layered media*, vol. 16, Elsevier, 2012.
- [12] R. L. Higdon, "Absorbing boundary conditions for acoustic and elastic waves in stratified media", *Journal of Computational Physics* **101** (1992), no. 2, p. 386-418.
- [13] A. H. Nayfeh, *Wave propagation in layered anisotropic media: With application to composites*, Elsevier, 1995.
- [14] H. Hellsten, V. Maz'ya, B. Vainberg, "The spectrum of water waves produced by moving point sources, and a related inverse problem", *Wave motion* **38** (2003), no. 4, p. 345-354.
- [15] O. V. Motygin, "On the statement of the three-dimensional Neumann-Kelvin problem", in *2008 Proceedings of the International Conference Days on Diffraction*, June 2008, p. 140-146.
- [16] P. Destuynder, C. Fabre, "A discussion on Neumann-Kelvin's model for progressive water waves", *Applicable Analysis* **90** (2011), no. 12, p. 1851-1876.
- [17] M. Bonnet, *Boundary integral equation methods for solids and fluids*, no. BOOK, John Wiley, 1995.
- [18] P. Bettess, "Infinite elements", *International Journal for numerical methods in engineering* **11** (1977), no. 1, p. 53-64.
- [19] R. Astley, "Infinite elements for wave problems: a review of current formulations and an assessment of accuracy", *International Journal for Numerical Methods in Engineering* **49** (2000), no. 7, p. 951-976.
- [20] B. Engquist, A. Majda, "Absorbing boundary conditions for numerical simulation of waves", *Proceedings of the National Academy of Sciences* **74** (1977), no. 5, p. 1765-1766.
- [21] L. Halpern, "Absorbing boundary conditions for the discretization schemes of the one-dimensional wave equation", *Mathematics of Computation* **38** (1982), no. 158, p. 415-429.
- [22] T. Hagstrom, "Radiation boundary conditions for the numerical simulation of waves", *Acta numerica* **8** (1999), p. 47-106.
- [23] E. Bécache, D. Givoli, T. Hagstrom, "High-order absorbing boundary conditions for anisotropic and convective wave equations", *Journal of Computational Physics* **229** (2010), no. 4, p. 1099-1129.
- [24] E. Bécache, A. B.-B. Dhia, G. Legendre, "Perfectly matched layers for the convected Helmholtz equation", *SIAM Journal on Numerical Analysis* **42** (2004), no. 1, p. 409-433.
- [25] J.-P. Berenger, "A perfectly matched layer for the absorption of electromagnetic waves", *Journal of computational physics* **114** (1994), no. 2, p. 185-200.
- [26] A. Bermúdez, L. Hervella-Nieto, A. Prieto, R. Rodri *et al.*, "An optimal perfectly matched layer with unbounded absorbing function for time-harmonic acoustic scattering problems", *Journal of Computational Physics* **223** (2007), no. 2, p. 469-488.
- [27] R. L. Higdon, "Absorbing boundary conditions for acoustic and elastic waves in stratified media", *Journal of Computational Physics* **101** (1992), no. 2, p. 386-418.
- [28] D. Givoli, *Numerical methods for problems in infinite domains*, vol. 33, Elsevier, 2013.
- [29] I. Harari, "A survey of finite element methods for time-harmonic acoustics", *Computer methods in applied mechanics and engineering* **195** (2006), no. 13-16, p. 1594-1607.
- [30] S. Ham, K.-J. Bathe, "A finite element method enriched for wave propagation problems", *Computers & structures* **94** (2012), p. 1-12.
- [31] P. Destuynder, C. Fabre, "Modélisation du comportement hydrodynamique des bateaux", Lecture, Jun 2012.
- [32] L. Rayleigh, "The form of standing waves on the surface of running water", *Proceedings of the London Mathematical Society* **1** (1883), no. 1, p. 69-78.
- [33] J.-M. Vanden-Broeck, F. Dias, "Gravity-capillary solitary waves in water of infinite depth and related free-surface flows", *Journal of Fluid Mechanics* **240** (1992), p. 549-557.
- [34] O. M. Phillips, *The dynamics of the upper ocean*, CUP Archive, 1966.
- [35] C. Geuzaine, J.-F. Remacle, "Gmsh: A 3-D finite element mesh generator with built-in pre-and post-processing facilities", *International journal for numerical methods in engineering* **79** (2009), no. 11, p. 1309-1331.
- [36] Y. Renard, K. Poullos, "GetFEM: Automated FE modeling of multiphysics problems based on a generic weak form language", *ACM Transactions on Mathematical Software (TOMS)* **47** (2020), no. 1, p. 1-31.
- [37] J. Ahrens, B. Geveci, C. Law, "Paraview: An end-user tool for large data visualization", *The visualization handbook* **717** (2005), no. 8.
- [38] F. Ihlenburg, I. Babuška, "Finite element solution of the Helmholtz equation with high wave number Part I: The h-version of the FEM", *Computers & Mathematics with Applications* **30** (1995), no. 9, p. 9-37.
- [39] F. Ihlenburg, *Finite element analysis of acoustic scattering*, vol. 132, Springer Science & Business Media, 2006.
- [40] P. Destuynder, C. Fabre, "Singularities occurring in multimaterials with transparent boundary conditions", *Quarterly of Applied Mathematics* **74** (2016), no. 3, p. 443-463.

- [41] J. M. Melenk, I. Babuška, “The partition of unity finite element method: basic theory and applications”, *Computer methods in applied mechanics and engineering* **139** (1996), no. 1-4, p. 289-314.
- [42] O. Laghrouche, P. Bettess, R. Astley, “Modelling of short wave diffraction problems using approximating systems of plane waves”, *International Journal for Numerical Methods in Engineering* **54** (2002), no. 10, p. 1501-1533.